Strategic Roles of Axial Histidines in Structure Formation and Redox Regulation of Tetraheme Cytochrome c_3[†]

Yuki Takayama,[‡,§,||] Nicolas D. Werbeck,[‡,⊥] Hirofumi Komori,[▽,+] Kumiko Morita,[▽] Kiyoshi Ozawa,[○,#] Yoshiki Higuchi,[▽,+] and Hideo Akutsu*[,‡]

Institute for Protein Research, Osaka University, 3-2 Yamadaoka, Suita, Osaka 565-0871, Japan, Institute for Bioinformatics Research and Development, Japan Science and Technology Agency, 5-3 Yonbancho, Chiyoda, Tokyo 102-8666, Japan, Graduate School of Life Science, University of Hyogo, Koto, Kamigori, Hyogo 678-1297, Japan, The RIKEN SPring-8 Center, 1-1-1 Koto, Sayo-cho, Sayo-gun, Hyogo 679-5248, Japan, and Faculty of Engineering, Yokohama National University, Hodogaya-ku, Yokohama 240-8501, Japan

Received April 2, 2008; Revised Manuscript Received July 18, 2008

ABSTRACT: Tetraheme cytochrome c_3 (cyt c_3) exhibits extremely low reduction potentials and unique properties. Since axial ligands should be the most important factors for this protein, every axial histidine of *Desulfovibrio vulgaris* Miyazaki F cyt c_3 was replaced with methionine, one by one. On mutation at the fifth ligand, the relevant heme could not be linked to the polypeptide, revealing the essential role of the fifth histidine in heme linking. The fifth histidine is the key residue in the structure formation and redox regulation of a *c*-type cytochrome. A crystal structure has been obtained for only H25M cyt c_3. The overall structure was not affected by the mutation except for the sixth methionine coordination at heme 3. NMR spectra revealed that each mutated methionine is coordinated to the sixth site of the relevant heme in the reduced state, while ligand conversion takes place at hemes 1 and 4 during oxidation at pH 7. The replacement of the sixth ligand with methionine caused an increase in the reduction potential of the mutated heme of 222−244 mV. The midpoint potential of a triheme H52M cyt c_3 is higher than that of the wild type by ∼50 mV, suggesting a contribution of the tetraheme architecture to the lowering of the reduction potentials. The hydrogen bonding of Thr24 with an axial ligand induces a decrease in reduction potential of ∼50 mV. In conclusion, the bis-histidine coordination is strategically essential for the structure formation and the extremely low reduction potential of cyt c_3.

Cytochrome c_3 (cyt c_3)[1] isolated from sulfate-reducing bacteria is a periplasmic electron transport protein whose molecular mass is typically ∼14 kDa, and it possesses four hemes attached to a single polypeptide. It is involved in sulfate respiration, which is the prototype of the oxygen respiration system. Because of its unusual properties, it is classified as a class III *c*-type cytochrome (*1*). The roles of the four hemes in regulation of the electron transport pathway in sulfate respiration are biologically relevant. The three-dimensional structures of ferrous and ferric cyt c_3 from various strains have been determined by means of X-ray crystallography and nuclear magnetic resonance spectroscopy (NMR) (*2* and references cited therein). Although the degree of sequence homology among cyt c_3 species is not high (∼30%), the heme architecture and the fold of the protein are conserved. The fifth and sixth ligands of each heme are histidines (His or H). Cyt c_3 has a variety of interesting properties (*3*). The most important of them is its extremely low reduction potentials. This can be attributed to the long history of sulfate respiration during biological evolution. The low potentials mean that cyt c_3 carries highly reductive heme irons. Its tetraheme architecture was suggested to be important for regulating redox processes (*3*). It is also known that a dried film of it becomes electric conductive on reduction (*4*). Therefore, this protein is intriguing not only from a biological point of view but also from physical and chemical ones.

Different from the monoheme cyt *c* involved in oxidative phosphorylation, cyt c_3 has two types of heme-binding motifs, namely, -Cys-(Xaa-)$_2$-Cys-His- and -Cys-(Xaa-)$_4$-Cys-His- (CXXXXCH), where Cys (C) and Xaa (X) are cysteine and

[†] This research was partly supported by a Grant-in-Aid for Scientific Research on Priority Areas from the Ministry of Education, Science, Technology, Sport and Culture of Japan to H.A., a grant from the Institute for Bioinformatics Research and Development to H.A. and Y.T., and a grant from The National Project on Protein Structural and Functional Analyses to Y.H.

* To whom correspondence should be addressed. Phone: +81-6-6872-8218. Fax: +81-6-6872-8219. E-mail: akutsu@protein.osaka-u.ac.jp.

[‡] Osaka University.

[§] Japan Science and Technology Agency.

[||] Current address: Department of Biochemistry and Molecular Biology, University of Texas Medical Branch, Galveston, TX 77555.

[⊥] Current address: Department of Biomolecular Mechanisms, Max Planck Institute for Medical Research, Heidelberg, Germany.

[▽] University of Hyogo.

[+] The RIKEN SPring-8 Center.

[○] Yokohama National University.

[#] Current address: Research School of Chemistry, Australian National University, Canberra, Australia.

[1] Abbreviations: cyt c_3, cytochrome c_3; *Dv*MF, *Desulfovibrio vulgaris* Miyazaki F; *Dv*H, *D. vulgaris* Hildenborough; CD, circular dichroism; MPOH, 3-mercapto-1-propanol; NMR, nuclear magnetic resonance; NaP_i, sodium phosphate buffer; L_5^n or L_6^n mutant, mutant with the fifth or sixth ligand, respectively, of heme *n* changed; Ccm, cytochrome *c* maturation system; SAM, self-assembled monolayer.

10.1021/bi8005708 CCC: $40.75
Published on Web 08/15/2008

any amino acid, respectively, and His is the fifth ligand. A classification of the cyt c_3 subfamilies based on the combination of heme binding motifs has been reported (*5*). The reduction potentials of the four hemes were found to be lower for the 2-4-2-4 subfamily than for other subfamilies. The potentials are in the ranges of −200 to −380 mV (*6*−*10*) and −90 to −355 mV (*11, 12*), respectively. The name of each subfamily is based on the number of Xaa residues in the four heme-binding motifs from the N-terminus to the C-terminus. Cyt c_3 from *Desulfovibrio vulgaris* Miyazaki F (*Dv*MF), the subject of this work, belongs to the 2-4-2-4 subfamily. Its macroscopic and microscopic reduction potentials have been determined, using differential pulse polarography and NMR (*13, 14*). Its oxidized (*15, 16*) and reduced (*2*) structures have been reported. Since an efficient overexpression system for cyt c_3 has been established (*17*), we have carried out a series of mutation works (*3*). This is one of the best-characterized cyt c_3 species. Using this system, we have tried to elucidate the significance of the bis-imidazole coordination and the tetraheme architecture. Although it is well-known that the reduction potential of the His−His coordinations is much lower than that of methionine (Met or M)−His coordinations (*18*), it is important to determine the actual values to understand the redox properties of cyt c_3. For this purpose, the axial His residues were replaced with Met one by one in this work. Mutations at the sixth axial ligand in *Desulfovibrio vulgaris* Hildenborough (*Dv*H) have been reported previously (*7, 8*). However, extensive work has not been carried out because of the difficulty with overexpression. In particular, heme-specific reduction potentials were not investigated. This has been done in this work. Furthermore, we could replace His not only at the sixth but also at the fifth coordination site. This work will also provide a complete view of the roles of the aromatic residues in cyt c_3, because we have mutated all noncoordinated aromatic residues in *Dv*MF cyt c_3 (*5, 16*). The results revealed that the axial histidine coordination is essential not only for realizing the extremely low reduction potentials but also for the structure formation of cyt c_3.

MATERIALS AND METHODS

Site-Directed Mutagenesis. All mutations were introduced into the pKFC3k plasmid, which contains the *Dv*MF cyt c_3 gene (*16*). Site-directed mutagenesis was performed with a Mutan-Super Express Km kit (Takara Bio Inc.), and synthetic oligonucleotides were purchased from QIAGEN. The synthetic oligonucleotides used in this study are summarized in Table 1. The mutations were confirmed by nucleotide sequencing with an ABI PRISM 310 genetic analyzer (Perkin-Elmer), using a DNA sequencing kit, BigDye Terminator Cycle Sequencing Ready Reaction version 1.0 (Applied Biosystems), and two M13 primers, RV-N and M4 (Takara Shuzo Co., Ltd.).

Cultivation and Purification. Mutated cyt c_3 species were expressed in *Shewanella oneidensis* TSP-C transformed with a mutated plasmid, as described previously (*17*). The [$C_\varepsilon{}^2H_3$]Met proteins were obtained in a medium comprising 31 mM sodium lactate, 31 mM disodium fumarate, 11 mM glucose, 10 mM sodium citrate, 93 mM NH_4Cl, 50 mM Na_2HPO_4, 22 mM KH_2PO_4, 12 mM NaCl, 500 μM $MgSO_4$, 100 μM $CaCl_2$, 20 μM $FeSO_4$, 1 μM $MnCl_2$, 20 mg/mL adenosine, 20 mg/mL guanosine, 20 mg/mL cytidine, 20 mg/mL thymidine, 20 mg/mL uridine, 20 mg/mL thiamine hydrochloride, 20 mg/mL α-biotin, and an amino acid mixture. The amino acid mixture (all per liter of culture) consisted of 300 mg of Ala, 200 mg of Arg, 400 mg of Asn, 400 mg of Asp, 50 mg of Cys, 400 mg of Gln, 1000 mg of Glu, 300 mg of Gly, 200 mg of His, 400 mg of Ile, 400 mg of Lue, 450 mg of Lys, 200 mg of Phe, 400 mg of Pro, 500 mg of Ser, 200 mg of Thr, 100 mg of Trp, 300 mg of Tyr, 300 mg of Val, and 150 mg of [d_3-methyl]Met (98% d_3-methyl, Cambridge Isotope Laboratories, Inc.). The pH was adjusted to 7.5. To obtain each mutant protein for this work, a 24−36 L, total, cell culture was used. The mutated cyt c_3 species were purified by the procedure used for the wild type (*19*). To prepare ferrous cyt c_3 forms, [NiFe] hydrogenese was purified from *Dv*MF cells according to the reported method (*20*).

Table 1: Synthetic Oligonucleotides Used for Site-Directed Mutagenesis[a]

mutation (ligand[b])	synthetic oligonucleotide
H34M ($L_5{}^1$)	5′(289)-GGC GAC TGT ATG CAC CCG GTC AAC-3′(312)
H52M ($L_5{}^2$)	5′(336)-C GCC ACC GCC GGT TGC ATG GAC AAC ATG G-3′(364)
H83M ($L_5{}^3$)	5′(433)-TGC GTG GGC TGC ATG CTT GAA ACC GCC-3′(459)
H106M ($L_5{}^4$)	5′(502)-GGC TCC AAG TGC ATG AGC TAA GAA TCC-3′(528)
H22M ($L_6{}^1$)	5′(250)-GTG GTC TTC AAC ATG TCG ACC CAC AAG-3′(276)
H35M ($L_6{}^2$)	5′(286)-TGT GGC GAC TGT CAT ATG CCG GTC AAC GCC-3′(315)
H25M ($L_6{}^3$)	5′(259)-AAC CAC TCG ACC ATG AAG GCC GTG AAG-3′(285)
H70M ($L_6{}^4$)	5′(393)-C TAC CAC GCC ATG ATG GAC AAG GGC ACC-3′(420)
H34K ($L_5{}^1$)	5′(285)-G TGT GGC GAC TGT AAG CAC CCG GTC AAC GG-3′(314)
H34Q ($L_5{}^1$)	5′(285)-G TGT GGC GAC TGT CAG CAC CCG GTC AAC GG-3′(314)
H34Y ($L_5{}^1$)	5′(285)-G TGT GGC GAC TGT TAC CAC CCG GTC AAC GG-3′(314)
T24V	5′(253)-GTC TTC AAC CAC TCG GTC CAC AAG GCC GTG-3′(282)

[a] The sequencing numbers in parentheses are the sequence numbers according to ref *16*. [b] $L_i{}^n$ stands for the *i*th ligand at heme *n*. H, M, K, Q, Y, T, and V stand for histidine, methionine, lysine, glutamine, tyrosine, threonine, and valine, respectively.

Mass Spectrometry. The mass number was determined with a matrix-assisted laser desorption ionization time-of-flight (MALDI-TOF) mass spectrometer (Autoflex, Bruker Daltonics). Cyt c_3 solutions were dialyzed against ultrapure water. Aliquots (1 μL) were deposited on an MTP 384 target plate of polished steel TF (Bruker Daltonics) followed by deposition of 1 μL of matrix, which comprised 10 mg/mL sinapinic acid (Bruker Daltonics) in 50% acetonitrile and 0.1% trifluoroacetic acid. Mass data were calibrated with Protein Calibration Standard I (Bruker Daltonics).

Circular Dichroism Measurements. Circular dichroism (CD) spectra were acquired with a Jasco J-720WI CD spectropolarimeter at 30 °C. The sample concentration for the far-UV region (190−250 nm) was 5 μM in 30 mM sodium phosphate buffer (NaP_i) (pH 7.0). The solvent spectrum obtained under the same conditions was subtracted.

CD spectra were recorded using a quartz cell with a path length of 1 mm.

Electrochemical Measurements. Differential pulse polarograms were recorded at 30 °C with a Perkin-Elmer 394 digital electrochemical trace analysis system (Perkin-Elmer) using a dropping mercury electrode and a Ag/AgCl reference electrode. The modulation amplitude, sweep rate, and drop time were 20 mV, 2 mV s^{-1}, and 2 s, respectively. To obtain macroscopic reduction potentials, the polarograms were fitted to an analytical equation for four and three consecutive one-electron reversible electrode reactions (*6*).

The reduction potentials of Met-coordinated hemes were determined with a 3-mercapto-1-propanol (MPOH)-coated gold electrode, using a computer-controlled three-electrode potentiostat (Hokuto Denko, HZ-5000). MPOH (Tokyo Chemical Ind. Ltd.) was used for preparation of the electrode without further purification. A mica sheet (Nilaco) was baked at 580 °C prior to the vapor deposition and maintained at 580 °C during the positioning of Au (99.99%). The substrates were then annealed at 530 °C for 8 h at ambient atmosphere to obtain large Au(III) terraces on the surface (*21*). SAM-MPOH-coated gold substrates were prepared by immersing Au-deposited mica substrates in a 1 mmol dm^{-3} ethanol solution of MPOH for 24 h. For voltammetry measurements, a substrate with SAM-MPOH was mounted at the bottom of a cone-shaped cell using an elastic O-ring (*22*). The surface area of the electrode was estimated to be 0.126 cm^2 from the diameter of the O-ring.

A solution of either 30 mM NaP_i (pH 7.0) or 30 mM borate buffer (pH 9.0) in a cell was deaerated via Ar bubbling for 15 min. Ten milligrams of cyt c_3 was then added to the cell (2 mg/mL), followed by dissolution with further Ar bubbling for less than 1 min. The reference electrode used was a Ag/AgCl/saturated KCl one equipped with a Vycor glass for the liquid junction. A platinum wire was used as the counter electrode. All voltammetry measurements were made at 21 ± 1 °C. At first, cyclic voltammograms were recorded at 100, 50, and 20 mV/s. Reversibility was confirmed for those at 50 and 20 mV/s. Then, polarograms were recorded at 20 mV/s. Reduction potentials are referred to the standard hydrogen electrode.

Nuclear Magnetic Resonance Measurements. Samples [1 mM cyt c_3 dissolved in 30 mM NaP_i (p^2H 7.0) or in 30 mM borate buffer (p^2H 9.0)] were prepared as described previously (*23*). Nuclear magnetic resonance (NMR) spectra at 500 and 600 MHz were recorded at 303 K with AVANCE DRX-500 and DRX-600 NMR spectrometers, respectively (Bruker Biospin). The size of the data set was 4096 × 512. The assignment of each heme in the fully reduced state and heme methyl signals in five macroscopic oxidation states was carried out as previously reported (*13, 14, 24*). Chemical shifts are presented in parts per million relative to 2,2-dimethyl-2-silapentane-5-sulfonate (DSS) as an internal reference.

Crystallization and Structure Determination. Crystals of H25M and T24V cyt c_3 were grown at 10 °C according to the method reported for the wild type (*25*). Here, H25M stands for the replacement of His25 with Met. T and V are threonine (Thr) and valine (Val), respectively; 150 μL of an H25M cyt c_3 solution [20 mg/mL, 10 mM borate buffer (pH 9.0)] containing 50% (v/v) 2-methyl-2,4-pentanediol (MPD) was equilibrated against 4 mL of the same buffer containing 70% MPD. In the case of T24V cyt c_3, 10 mM sodium phosphate buffer (pH 7.0) was used.

Table 2: Summary of X-ray Crystallographic Data

	H25M cyt c_3	T24V cyt c_3
X-ray source	Rigaku RA-Micro7	BL41XU, SPring-8
wavelength (Å)	1.541	0.71000
space group	$P2_12_12_1$	$P2_12_12_1$
unit cell parameters (Å)	$a = 51.94$, $b = 67.16$, $c = 34.57$	$a = 52.43$, $b = 67.54$, $c = 34.41$
resolution range (outer shell) (Å)	11.50−1.50 (1.58−1.50)	10−1.00 (1.04−1.00)
no. of measured reflections	122630	465200
no. of unique reflections	18745	61485
completeness (%)	94.1 (89.9)	99.3 (98.9)
R_{merge}	0.068 (0.243)	0.058 (0.303)
$\langle I/\sigma(I)\rangle$	8.9	13.9
R	0.178	0.109
R_{free}	0.195	0.140

Diffraction experiments were carried out at 100 K for H25M and T24V cyt c_3. The diffraction data set for H25M cyt c_3 was collected on an RAXIS-VII instrument (Rigaku Co. Ltd.) using Cu Kα radiation generated by a rotating anode (RA-Micro7). The data set for T24V cyt c_3 was collected using a synchrotron radiation source ($\lambda = 0.71$ Å) at the BL41XU beamline with a Quantum315 detector system at SPring-8. The crystal-to-detector distance was 200 mm (Quantum315) or 75 mm (RAXIS-VII) with an oscillation range per image of 1.0°. Integration of the reflections was performed using HKL2000 (*26*) for T24V cyt c_3 and MOSFLM (*27*) for H25M cyt c_3. Initial phase calculation and refinement for both mutants were carried out with CNS (*28*) using the atomic coordinates of the wild-type cyt c_3 without water molecules (*16*) as a starting model. The structures of T24V and H25M cyt c_3, including water molecules, were refined with isotropic B factors using CNS. The structure of T24V cyt c_3 was further refined with anisotropic B factors using SHLXL (*29*). The R values for the final models of H25M and T24V cyt c_3 were 0.178 and 0.122, respectively. The X-ray crystallographic data are summarized in Table 2. The root-mean-square deviation (rmsd) values for the backbone atoms were calculated with Swiss-Pdb Viewer 3.7 (*30*). The coordinates and structure factors for T24V and H25M cyt c_3 have been deposited in the Protein Data Bank as entries 2EWK and 2YXC, respectively.

RESULTS

Effect of Mutation of an Axial Ligand on Cyt c_3 Expression. To elucidate the role of an axial ligand, every axial His of *Dv*MF cyt c_3 was replaced with Met, one by one. The effects of the replacements were characterized by the yield, the ratio of absorbance at the α-band in the reduced state to that at 280 nm in the oxidized state ($A_\alpha^{red}/A_{280}^{ox}$), and the mass number, all results being summarized in Table 3. The yield of a mutant of the fifth ligand (L_5 mutant) was lower than that of the L_6 ones except for the heme 4 mutant. The heme content of each mutant was estimated on the basis of $A_\alpha^{red}/A_{280}^{ox}$. Although it was almost the same as that of the wild type for every L_6 mutant, it was reduced to 60−85% for every L_5 mutant. Additionally, the mass numbers of the L_5 mutants were reduced by ~610, which accounts for that of

Table 3: Characterization of Mutant Cyt c_3 Species as Axial Ligands

sample (ligand[a])	yield (mg/L of culture)	$A_\alpha^{red}/A_{280}^{ox}$[b]	mass number[c]
wild type	9.01	3.00	14056 (+12)
H34M (L_5^1)	0.04	1.94 (65%)	13440 (−610)
H52M (L_5^2)	0.88	2.55 (85%)	13437 (−613)
H83M (L_5^3)	0.03	2.31 (77%)	13438 (−612)
H106M (L_5^4)	0.79	2.43 (81%)	13437 (−610)
H22M (L_6^1)	0.85	2.88 (96%)	14066 (+16)
H35M (L_6^2)	4.76	2.98 (99%)	14048 (−2)
H25M (L_6^3)	4.76	2.92 (97%)	14046 (−4)
H70M (L_6^4)	0.71	2.94 (98%)	14053 (+3)
H34Q (L_5^1)	0.01	1.80 (60%)	13437 (−610)
H34K (L_5^1)	0.02	1.92 (64%)	13437 (−610)
H34Y (L_5^1)	0.02	1.94 (65%)	13472 (−610)

[a] L_i^n stands for the ith ligand at heme n. [b] The heme content estimated as the absorbance ratio is shown in parentheses, that for the wild type being 100%. [c] The difference (expected mass − observed mass) is given in parentheses. The standard errors are ±1%.

a single heme. It can be concluded that one heme is not linked to the polypeptide chain in the L_5 mutants, although the apparent heme content is 60−80%.

Since the number of covalent bonds between the coordinated $N_{\epsilon 2}$ and C_α atoms of His (four bonds) is larger by one than that between the S_δ and C_α atoms of Met (three bonds), H34Q (N_ε or O_ε), H34K (N_ζ), and H34Y (O_η) mutations were also introduced to maintain the chain length at the fifth coordination site (the expected coordinated atom being given in parentheses). Q, K, and Y stand for glutamine, lysine, and tyrosine, respectively. They exhibited similar results, which can be seen in Table 3. This indicates that no amino acid residues but His at this site can introduce covalent bonds between heme and Cys residues. Namely, only His in the heme-binding motif is recognized as the fifth ligand by the cytochrome *c* maturation system (Ccm) in *Shewanella* cells. This coincides with the observation that the *Escherichia coli* Ccm recognized only imidazole as the fifth ligand (*31*). In the case of *E. coli*, His in the CXXCH motif created in cyt b_{562} was replaced with Met, arginine, or Lys. In the case of a multiheme cytochrome *c* such as a cyt c_3, the maturation of the whole protein is not blocked by the inhibition of heme linking at one site, suggesting that the heme linking process at each heme-binding motif is independent. However, the lack of one heme significantly suppresses the efficiency of the protein production. The heme content should be 75% of that of the wild type, if L_5 mutants have only three hemes. However, it is in the range of 60−85%, suggesting the presence of a *b*-type heme, as in the case of *E. coli* (*31*). A lower value such as 60−65% can be ascribed to broadening of the band due to structural inhomogeneity. Thus, the preparations of L_5 mutants are inhomogeneous in terms of heme number and structure.

Structural characterization of all mutants was carried out by CD spectroscopy. The spectra are illustrated in Figure 1. There are only small changes in the secondary structure contents for the L_6 mutants, in accordance with the previous work on *Dv*H (*32*). In contrast, the secondary structure contents of the L_5 mutants were distinctly reduced. Nevertheless, the polypeptide could fold into a globular structure even with three hemes. Further characterizations of the L_5 mutants were not carried out because of their inhomogeneity in heme number and structure.

Coordination Structure at the Mutated Sites. To examine the effect of a mutation on its structure, we tried to crystallize

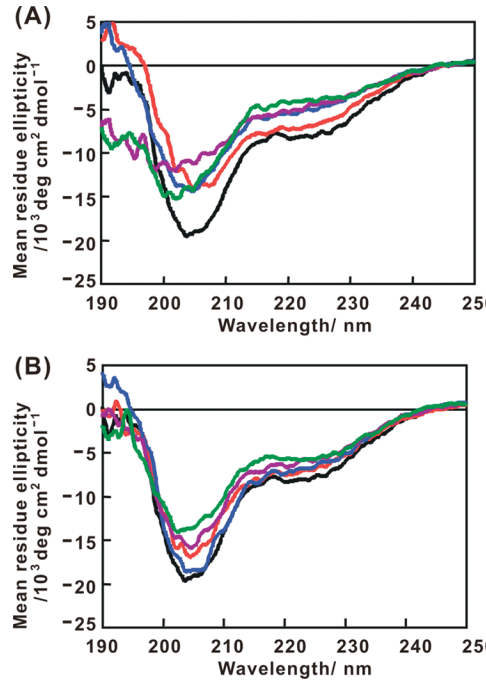

FIGURE 1: Circular dichroism spectra of H34M, H52M, H83M, and H106M cyt c_3 (A) and H22M, H35M, H25M, and H70M cyt c_3 (B) at pH 7.0. (A and B) Mutations at the fifth and sixth coordination sites, respectively. Black, red, blue, purple, and green show data for the the wild type and heme 1−4 axial ligand mutants, respectively.

every L_6 mutant. Since only ferric H25M(L_6^3) cyt c_3 was successfully crystallized at pH 9.0, its structure was determined (green in Figure 2A). L_6^3 stands for the L_6 mutant of heme 3. There was no significant difference in the polypeptide folding in comparison with that of the wild type (PDB entry 1J0O; red in Figure 2A). The rmsd value for the backbone atoms was 0.35 Å. The effect of the axial ligand replacement at heme 3 was local. The sixth ligand of heme 3 was S_δ of Met25, as expected (Figure 2B). The His$N_{\epsilon 2}$−iron (Fe) and MetS_δ−Fe distances at heme 3 were 1.99 and 2.34 Å, respectively. The S_δ−Fe length is consistent with those found in other cyt *c* species with Met−His coordinations. For instance, those for human and horse cyt *c* and *Saccharomyces cerevisiae* iso-1-cyt *c* are 2.38, 2.66, and 2.19 Å, respectively (PDB entries 1J3S, 1AKK, and 1YIC, respectively). It can be concluded that S_δ is the sixth ligand of H25M cyt c_3.

Then, coordinated atoms in the sixth axial ligands of other mutants were identified on the basis of one-dimensional ^{1}H NMR spectra of the ferrous forms at pH 9.0 (Figure 3). Since the coordinated Met80 $C_\varepsilon H_3$ signal of recombinant human cytochrome *c* appears at −3.28 ppm (BioMagResBank entry 5406), the signals indicated by black arrows in Figure 3 are candidates for the $C_\varepsilon H_3$ signal of the coordinated Met. To confirm the assignment, Met was specifically deuterated using [$C_\varepsilon{}^2H_3$]Met. The intensity of the tentatively assigned signal was significantly diminished on deuteration for every mutant (colored red in Figure 3). The Met coordination in the crystal structure of H25M cyt c_3 at pH 9.0 also justifies the assignment of the coordinated Met $C_\varepsilon H_3$ signals. This is also the case for the reduced mutants at pH 7.0, because similar signals were observed at pH 7.0 (spectra not shown).

^{1}H NMR spectra for the heme methyl signal regions of the fully oxidized cyt c_3 species are shown in Figure 4.

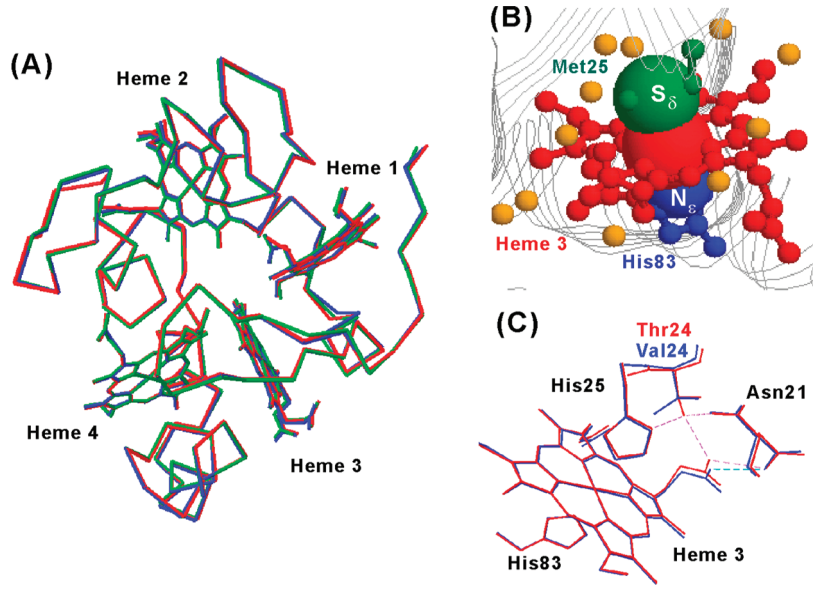

FIGURE 2: (A) Overall structures (backbone) and heme architectures of the wild-type (red), H25M (L_6^3) (green), and T24V (blue) cyt c_3 in crystal. (B) Crystal structure of H25M cyt c_3 around heme 3. The backbone, heme 3, His83 (fifth ligand), Met25 (sixth ligand), and water molecules within 10 Å of the Fe of heme 3 are represented as gray lines, and red, blue, green, and orange spheres, respectively. This figure was prepared with RasMol (*47*). (C) Comparison of the crystal structures of the wild-type (red) and T24V (blue) cyt c_3 around heme 3. The hydrogen bond in the wild type and that in the T24V mutant are colored pink and light blue, respectively. Panels A and C were prepared with Swiss-PdbViewer (*30*).

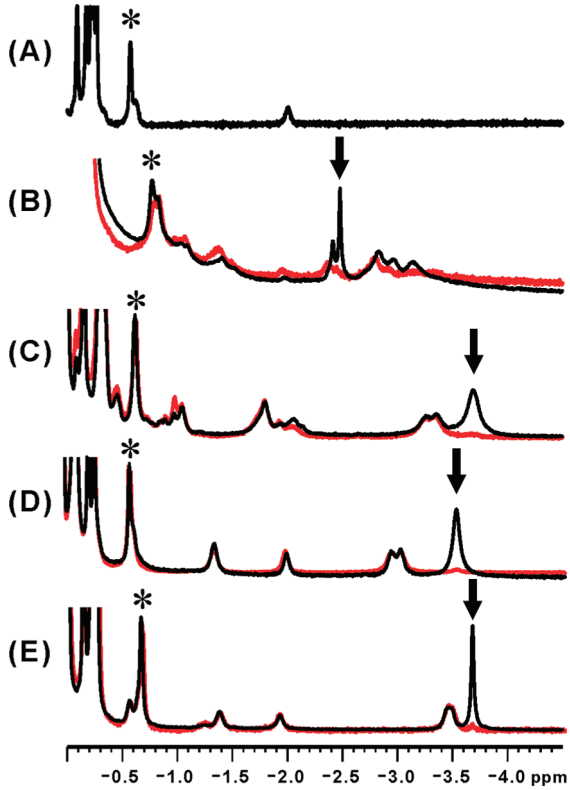

FIGURE 3: ^{1}H NMR spectra of wild-type (A), H22M (B), H35M (C), H25M (D), and H70M (E) ferrous cyt c_3 in a low-frequency region at p^{2}H 9.0, 600 MHz, and 303 K. All but spectrum A are L_6 mutants of hemes 1−4, respectively. The spectra of [$C_\varepsilon{}^2H_3$]Met-labeled proteins are superimposed on those of the relevant mutants in red. Asterisks and arrows indicate Ala68 βCH_3 and Met $C_\varepsilon H_3$ signals, respectively.

Typical low-spin spectra were observed at pH 9.0, as expected from Figure 3. In contrast, broad peaks appeared in the region from 35 to 60 ppm and at 39 ppm at p^{2}H 7.0 for H22M (L_6^1) and H70M (L_6^4) cyt c_3, respectively. This could be assigned to a high-spin or intermediate-spin state. A much smaller peak was also observed at ~40 ppm for the H35M (L_6^2) mutant. Although the low-spin state also prevails at p^{2}H 7.0, the molecular species are heterogeneous. The coordination structure can be examined in the lowest-frequency region (Figure 5). The coordinated His $C_{\delta 2}$ proton signals appear in this region (*33*). The coordinated Met $C_\varepsilon H_3$ signal of horse cytochrome *c* appears at −27.6 ppm (BioMagResBank entry 317) (*34*) due to a paramagnetic effect. In Figure 5, the spectra of nonlabeled (black) and [$C_\varepsilon{}^2H_3$]Met-labeled (red) L_6 mutants were superimposed. Coordinated Met $C_\varepsilon H_3$ signals can be seen at approximately −5.5 and −11.5 ppm for H25M and H35M ferric cyt c_3, respectively, at pH 7.0, and only for the H25M one at pH 9.0. The weaker paramagnetic effect, compared to that for horse cyt *c*, indicates that the coordination in solution is weaker in spite of a normal coordination bond length for H25M cyt c_3 in the crystal. Since the ligand at every mutated site is Met in the reduced state, the ligand should be replaced during oxidation for H22M, H35M, and H70M cyt c_3 at p^{2}H 9.0, and for H22M and H70M cyt c_3 at pH 7.0. In view of the low-spin state, a non-Met ligand in the oxidized state should be a strong one. However, there is no candidate amino acid residue in the proximity. An obvious candidate is a hydroxide ion. A small fraction of mutated hemes would be in the high-spin or intermediate-spin state, judging from Figure 4. The rate of exchange between different states is slow on the NMR time scale.

Redox Properties of L_6 Mutant Cyt c_3. Two-dimensional exchange spectra of L_6 mutants at different oxidation stages were recorded (spectra not shown). The assignment of heme methyl signals in the five macroscopic oxidation states was carried out as previously reported (*13, 14, 24*). The reduction fractions (R_i^j, where *i* and *j* are the heme number and *j*th reduction step, respectively) were calculated using the chemical shifts of signals 2- and 18-CH_3 for heme 1, 7- and

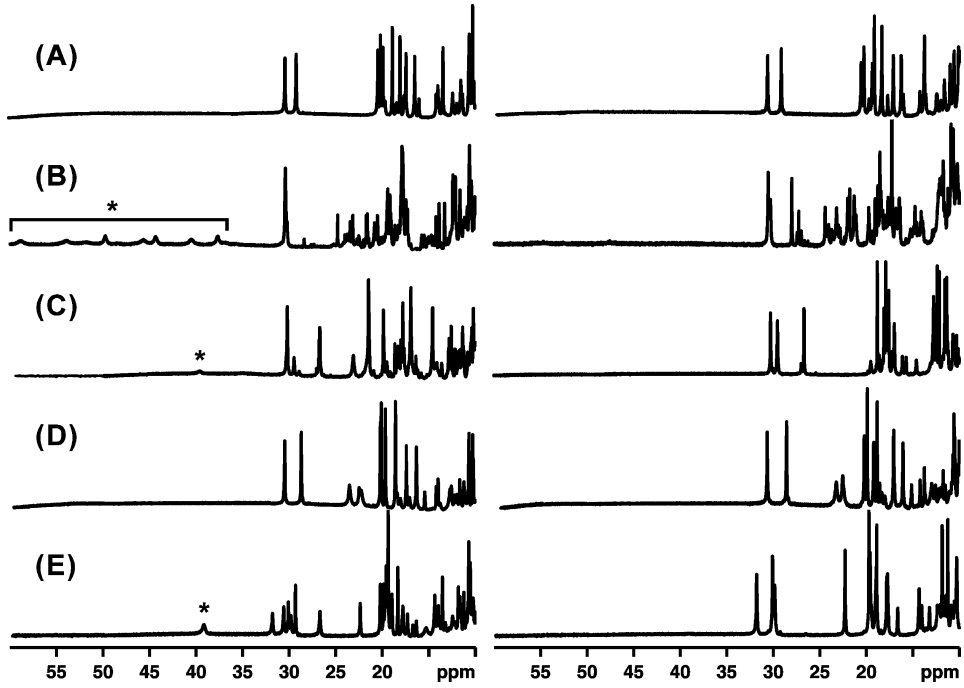

FIGURE 4: ^{1}H NMR spectra of wild-type (A), H22M (B), H35M (C), H25M (D), and H70M (E) ferric cyt c_3 at 600 MHz and 303 K: (left) p^{2}H 7.0 and (right) p^{2}H 9.0. Only the fingerprint regions for heme methyl groups are presented. Asterisks indicate putative high- or intermediate-spin species.

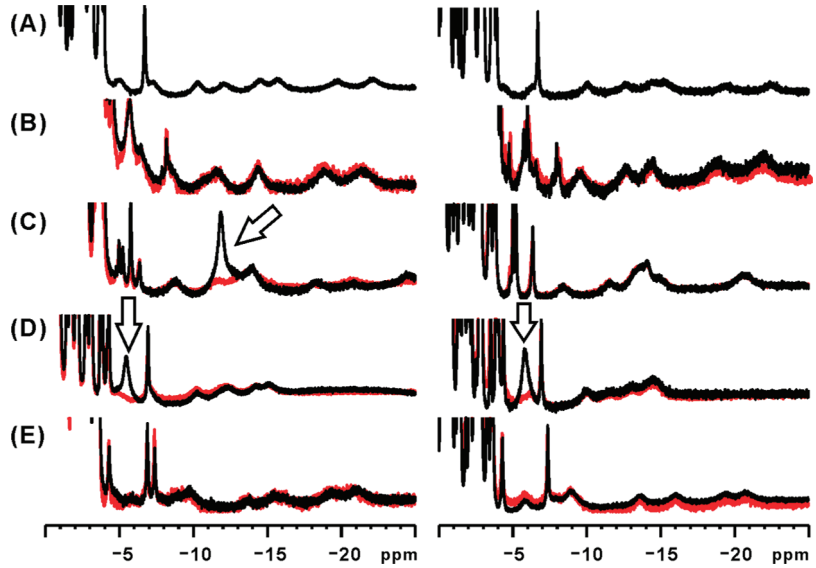

FIGURE 5: ^{1}H NMR spectra of wild-type (A), H22M (B), H35M (C), H25M (D), and H70M (E) ferric cyt c_3 in a low-frequency region at 600 MHz and 303 K: (left) p^{2}H 7.0 and (right) p^{2}H 9.0. The spectra of [$C_\varepsilon{}^2H_3$]Met-labeled proteins are superimposed on those of the relevant mutants in red. Arrows indicate Met $C_\varepsilon H_3$ signals.

18-CH_3 for heme 2, 12- and 18-CH_3 for heme 3, and 2- and 18-CH_3 for heme 4 (*5*), which are summarized in Table S1 of the Supporting Information. The reduction fractions of H22M ($L_6{}^1$) and H70M ($L_6{}^4$) cyt c_3 were obtained at only pH 9.0 because there were at least two molecular species at pH 7.0 (Figure 4). The methyl chemical shifts of the mutated heme could not be directly assigned for every mutant because of the slow exchange. In this case, its reduction fraction was estimated by calculation under the condition of $\sum_i R_l^i = 1$. The obtained average R_l^i values are presented in Table S2 of the Supporting Information. In every case, the mutated heme was responsible for the first reduction step (nearly 90% reduction in R^1).

At first, we tried to determine the four macroscopic reduction potentials by measuring a differential pulse polarogram (DPP) with a mercury electrode. The observed DPPs are presented in Figures 6 and S1 (Supporting Information). The fitting of experimental data was carried out as described in Materials and Methods. However, the macroscopic reduction potentials obtained with the assumption of four consecutive one-electron reversible electrode reactions contradicted the reduction fractions obtained via NMR. The Met coordination structure might be susceptible to the interaction with the mercury electrode. A MPOH-coated gold electrode was utilized, because it should prevent a direct metal−protein interaction. Actually, responses were

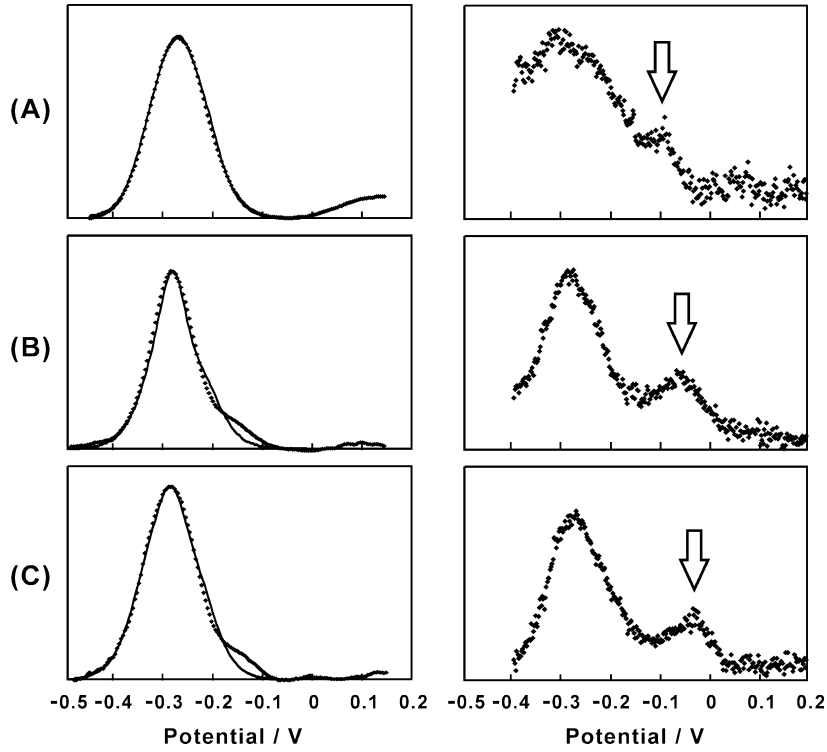

FIGURE 6: Differential pulse polarograms and voltammograms (DPPs and DPVs, respectively) of H35M (L_6^2) (A) and H25M (L_6^3) (B and C) cyt c_3 at pH 7.0 (A and B) and pH 9.0 (C). Left and right panels show data for DPPs and DPVs, respectively. The squares represent experimental data, and the lines are the best-fit theoretical curves. The arrows indicate responses ascribed to the Met-coordinated heme. The potentials are referred to the standard hydrogen electrode.

Table 4: Four Macroscopic Reduction Potentials of the Wild-Type and Mutated Cyt c_3 Species in 30 mM Sodium Phosphate Buffer (pH 7.0) or 30 mM Borate Buffer (pH 9.0) at 30 °C

sample (ligand[a])	$E_I^{\circ\prime}$[b]	$E_{II}^{\circ\prime}$	$E_{III}^{\circ\prime}$	$E_{IV}^{\circ\prime}$
		pH 7.0		
wild type[c]	−242	−296	−313	−358
H22M (L_6^1)	nd[d]	−220 (+76)	−242 (+71)	−297 (+61)
H35M (L_6^2)	−95 (+147)	−240 (+56)	−285 (+28)	−331 (+27)
H25M (L_6^3)	−63 (+179)	−240 (+56)	−293 (+20)	−315 (+43)
H70M (L_6^4)	nd[d]	−210 (+86)	−269 (+44)	−312 (+46)
T24V	−221 (+21)	−273 (+23)	−305 (+8)	−340 (+18)
		pH 9.0		
wild type	−240	−292	−324	−363
H22M (L_6^1)	nd[d]	−210 (+82)	−238 (+87)	−296 (+67)
H35M (L_6^2)	nd[d]	−230 (+62)	−297 (+27)	−337 (+26)
H25M (L_6^3)	−41 (+199)	−240 (+52)	−301 (+23)	−339 (+24)
H70M (L_6^4)	nd[d]	−210 (+82)	−259 (+65)	−312 (+51)

[a] L_i^n stands for the ith ligand at heme n. [b] $E_i^{\circ\prime}$ (i = I−IV) is the macroscopic reduction potential at the ith reduction step relative to the standard hydrogen electrode (SHE). The standard errors are ±2 mV. The differences (mutant − wild type) are given in parentheses. [c] From ref *16*. [d] Not determined.

observed at approximately −100 and −50 mV in the differential pulse voltamograms (DPVs) of H35M (L_6^2) and H25M (L_6^3) cyt c_3, respectively, as shown in Figure 6. They were also observed in the cyclic voltammograms (CVs, Figure S2). DPV of the buffer exhibited no signals in the relevant region (Figure S1), showing that the responses originated from the sample proteins. There is no macroscopic reduction potential in this potential range for the wild type (Table 4), and actually no response was observed in its DPV (not shown). These observations led to the assignment of the minor response to the Met-coordinated heme. Such a response, however, was not observed for the other L_6 mutants (Figure S1), presumably due to the ligand conversion.

To analyze these data, we have to characterize the species responsible for the DPVs and DPPs. The peak current of CV measured with the MPOH-coated gold electrode is a linear function of the square root of the scan rate as shown in Figure S2 for all mutant cyt c_3 species at pH 9.0. This is the case not only for the major peak but also for the minor one, revealing that the species responsible for their electrochemical processes at the electrode are freely diffusing proteins. Furthermore, they should take on the intact structures, because every Met is coordinated to the heme in the potential range of interest as we will show below, and the structure of the Met-coordinated protein should be similar to that of the wild type in view of the crystal structure and CD and NMR spectra described above. The minor response was observed for only H35M (pH 7.0) and H25M (pH 7.0 and 9.0) cyt c_3, which maintain the Met coordination throughout the redox process. In the potential range of the major response, every mutated heme should be reduced, since the reduction potential of the mutated heme is the highest among those of the four hemes as shown in the NMR results. We have shown that Met is coordinated to the heme in the reduced state at pH 9.0 and 7.0.

The DPP response curves are similar to the major response curves in DPV which can be seen in Figure 6 and Figure S1, revealing that they represent the same electrochemical processes. Therefore, the DPP responses should also come from the three nonmutated hemes of the freely diffusing intact proteins. The competence of the three nonmutated hemes was verified in the DPV experiments with H22M and H70M cyt c_3 (Figure S2). In view of these results, the polarograms were fitted to the three consecutive one-electron

Table 5: Microscopic Reduction Potentials at the First and Fourth Reduction Steps (e_i^{I} and e_i^{IV} for heme *i*, respectively) at pH 7.0 or 9.0 and 30 °C[a]

pH 7.0				
sample	e_1^{I}	e_2^{I}	e_3^{I}	e_4^{I}
wild type[b]	−308	−325	−286	−252
H35M (L_6^2)[c]	nd[d]	−97 (+228)	nd[d]	nd[d]
H25M (L_6^3)	nd[d]	nd[d]	−64 (+222)	nd[d]
T24V	−294 (+14)	−332 (−7)	−236 (+50)	−247 (+5)
	e_1^{IV}	e_2^{IV}	e_3^{IV}	e_4^{IV}
wild type	−293	−315	−344	−308
H35M (L_6^2)	−295 (−2)	nd[d]	−316 (+28)	−281 (+27)
H25M (L_6^3)	−277 (+16)	−295 (+20)	nd[d]	−285 (+23)
T24V	−285 (+8)	−319 (−4)	−291 (+53)	−307 (+1)
pH 9.0				
	e_1^{I}	e_2^{I}	e_3^{I}	e_4^{I}
wild type	−309	−323	−286	−248
H25M (L_6^3)	nd[d]	nd[d]	−42 (+244)	nd[d]
	e_1^{IV}	e_2^{IV}	e_3^{IV}	e_4^{IV}
wild type[b]	−297	−330	−345	−307
H25M (L_6^3)	−308 (−11)	−323 (+7)	nd[d]	−295 (+12)

[a] The differences (mutant − wild type) are given in parentheses. [b] Recalculated from the data reported in ref *14*. [c] L_i^n stands for the *i*th ligand at heme *n*. [d] Not determined.

reversible electrode reactions (*6*). These macroscopic potentials can be ascribed to the Met-coordinated proteins as mentioned above. The obtained values are summarized in Table 4. A small shoulder found at approximately −0.13 V in the differential pulse polarograms of Figure 6 may be due to the denatured cyt c_3 adsorbed on the mercury surface. Although there are minor species for H22M and H70M cyt c_3 at pH 7.0, the observed DPPs and DPVs should represent the electrochemical reactions of the major low-spin species.

To clarify the effect of mutation on each heme, the microscopic reduction potentials were determined from the macroscopic reduction potentials and the reduction fractions (*14*) for H35M and H25M cyt c_3, in which Met is stably coordinated during the redox process. Their microscopic reduction potentials at the first reduction step (e^{I}) and the fourth reduction step (e^{IV}) could be determined without any assumption. The former and the latter are those between the fully oxidized (S_o) and one-electron-reduced (S_1) states and between the three-electron-reduced (S_3) and fully reduced (S_4) states, respectively. They are summarized in Table 5. The reduction potentials of the relevant heme increased by 222−244 mV.

Structural and Redox Properties of T24V Cyt c₃. $H_{\delta 1}$ of His25 (sixth ligand of heme 3) is involved in hydrogen bonding with the carbonyl oxygen of asparagine 21 and O_γ of Thr24 in the oxidized state (*16*), while the latter is lost in the reduced state (*2*). The crystal structure of T24V *Dv*MF cyt c_3 was determined at 1.0 Å resolution and is presented in panels A and C of Figure 2. It was similar to that of the wild type except for the mutated region. Therefore, the effect of the mutation on reduction potentials could be ascribed to elimination of the hydrogen bond with Thr24. The microscopic reduction potentials were calculated from reduction fractions (Table S2 of the Supporting Information) and macroscopic reduction potentials (Table 4) and are included in Table 5. The effect of the mutation was largest for heme 3, e_3^{I} and e_3^{IV} increasing by 50 and 53 mV, respectively. Those for *Dv*H T24V cyt c_3 were 75 and 106 mV, respectively (*35*). These results indicate that Thr24 makes heme 3 the most effective electron donor in the reduced state with the lowest e^{IV}.

DISCUSSION

Two thioether linkages and the fifth axial His are the basic features of *c*-type cytochromes (*18, 36*). The essential role of the latter in formation of the former has been revealed for a genuine *c*-type and multiheme cytochrome gene in this work. We can conclude that the fifth axial His is essential not only for the redox regulation but also for the heme linking to *c*-type apocytochromes in *S. oneidensis* as well as in *E. coli* (*31*). There are three distinct types of Ccms, namely, types I, II, and III (*36*). The Ccms of *S. oneidensis* and *E. coli* are classified as type I. Since the *D. vulgaris* Ccm is also classified as type I (*37*), His should play the same role in the maturation of cyt c_3 in sulfate-reducing bacteria. A mechanism for the His recognition has been proposed on the basis of the crystal structure of *B. subtilis* ResA (a component of a type II Ccm) (*38*), where a special cavity called "a histidine clamp" was assumed to recognize His in the heme-binding motif (*38*). ResA exhibits a high degree of homology to CcmG of *E. coli* in terms of amino acid sequence (30% identical) (*39*). Thus, the involvement of the fifth axial His in heme linking would be a general mechanism in Ccms. Furthermore, since not only His in CXXCH but also that in CXXXXCH is recognized as the essential residue for heme linking, Ccm should be originated earlier than the establishment of oxygen respiration. Although the heme linking takes place independently among the four hemes in cyt c_3, the formation of the heme architecture seems to be important for protein folding (*40*).

The effects of the L_6 mutations on the reduction potentials were significant for hemes 1 and 4 because their sixth ligands are converted during the redox process. It has been reported that the protein structure becomes more compact in the reduced state than in the oxidized state (*2*). This compactness would stabilize the Met coordination in the reduced state. In particular, conformational changes take place at the interfaces between hemes 1 and 2 and between hemes 2 and 4 during the oxidation. The effect of the conformational change should be smallest for heme 3. Furthermore, the environment around the sixth ligand of heme 3 may be flexible enough to adapt to the replacement of His with Met even in the oxidized state. A protein structure without Met coordination has less secondary structure and is less stable. The reduction fraction of H22M cyt c_3 (Table S2 of the Supporting Information) indicates that the order of the major reduction changed from hemes 4 → 1 → 2 → 3 to hemes 1 → 3 → 2 → 4 on mutation. In view of the similar secondary structure for wild-type and H22M cyt c_3 (Figure 1), the changes in the reduction potentials for all hemes should be due to a modification of the heme architecture.

To confirm the effect of the heme architecture on the reduction potentials, a differential pulse polarogram of the triheme architecture of H52M (L_5^2) cyt c_3 (Figure S3 of the Supporting Information) was obtained. It showed an increase in the midpoint potential by ∼50 mV compared to that for the wild-type tetraheme cyt c_3, supporting the

contribution of the tetraheme architecture to the lowering of the reduction potentials. A similar tendency was also observed for cyt c_3-like natural triheme cytochrome *c* species (cyt c_7 and PpcA). The midpoint potentials of those from *Desulfuromonas acetoxidans* and *Geobacter sulfurreducens* are −181 (*41*) and −146 mV (*42*), respectively.

The microscopic reduction potentials of *Dv*MF cyt c_3 are pH-dependent in the neutral-pH region. However, the pK_a of propionate would not be affected directly by the replacement of an axial ligand because the behaviors of the heme methyl chemical shifts for H35M (L_6^2) and H25M (L_6^3) cyt c_3 between pH 7.0 and 9.0 were similar to those of the wild type (Figure 4 and Table S1 of the Supporting Information). Therefore, we can discuss the changes in the reduction potentials as the effects of the mutations. The most significant effect on the reduction potential of each heme was found for the mutated heme. The increases in e_3^I of H25M cyt c_3 on replacement with Met were 222 and 244 mV at pH 7.0 and 9.0, respectively (Table 5). This is similar to the increase in the e_2^I of H35M cyt c_3 at pH 7.0 (228 mV). In the case of *Dv*H cyt c_3, an isolated weak response was observed at −90 and −65 mV for H25M and H70M cyt c_3, respectively (*7, 8*). Although the microscopic reduction potentials were not determined, the increases in e_3^I and e_4^I may be similar to those of *Dv*MF cyt c_3, judging from their highest macroscopic reduction potential. It should be noted that the Met-coordinated hemes are different for *Dv*MF and *Dv*H cyt c_3. In the case of monoheme cyt *c* species, the replacement of the sixth axial Met with His reduced the reduction potentials, $\Delta E^{\circ\prime}$, by 221, 390, and 205 mV in the cases of M80H horse mitochondrial cyt *c* (*18*), M78H *Aquifex* cyt c_{555} (*43*), and M61H *Pseudomonas* cyt c_{551} (*44*), respectively. The reported data indicate that the observed increase in the reduction potential induced by the replacement of His with Met in *Dv*MF cyt c_3 is reasonable, although the observed potential itself is still much lower than those of mitochondrial cyt *c* species.

On the basis of this work and the investigations reported so far, we can summarize the factors contributing to the extremely low reduction potentials of *Dv*MF cyt c_3 in comparison with a mitochondrial cyt *c* (∼560 mV higher than the midpoint potential of cyt c_3). As shown in this work, bis-histidine coordination decreases the reduction potentials by more than 220 mV with respect to the Met−His coordination. The higher degree of heme exposure in cyt c_3 (∼17%) is a well-known contribution (*16*). With simple estimation (*45*), one can expect a ∼180 mV decrease in comparison with the reduction potential of a mitochondrial cyt *c* (4% exposure). The quadrilateral tetraheme architecture of cyt c_3 is another factor. The increase in the midpoint potential for a chain tetraheme architecture (small tetraheme cyt *c*) is more than 100 mV in comparison with that of cyt c_3 (*46*). This would be based on the difference in the mode of interheme interaction. We may regard ∼100 mV as a global effect based on the heme architecture. These contributions account for ∼500 mV out of 560 mV. In addition, hydrogen bonding with an axial ligand and an aromatic $\pi-\pi$ interaction with the axial imidazole (*5*) decrease the reduction potential of a particular heme by 40−50 mV.

CONCLUSION

The fifth axial His was found to be directly involved in the heme linking in the process of maturation of *c*-type cytochromes. The three heme attachment sites (two thioether linkages and the fifth ligand) in the heme-binding motif CX_nCH ($n = 2-4$) yield a well-defined orientation of a heme in the protein. The sixth coordination will fix the folding of the polypeptide and refine the heme orientation. Since most *c*-type cytochromes are involved in electron transport, the fixed heme orientation should be important for the efficient electron transfer with a redox partner. This kind of heme-fixing device must have been particularly important for a small protein or a multiheme protein at an early stage of evolution, because the polypeptide was not long enough to stabilize its folding and heme cavity on its own. Thus, the fifth His was incorporated into the cytochrome *c* maturation reaction at the time of an anaerobic atmosphere, to which cyt c_3 can be traced back. This resulted in the evolutional conservation of the heme-binding motif. Consequently, the fifth His became a strategically essential residue for *c*-type cytochromes. Bis-imidazole coordination at the heme iron could provide the best redox center for electron transport in a reduced environment because of its extremely low reduction potential. Then, the sixth ligand and protein environment were used for diversification of the electron transport system and for adapting to the oxidization of the atmosphere. To keep the reduction potential extremely low, the sixth axial His is also essential for cyt c_3.

ACKNOWLEDGMENT

We thank Ms. Fumiko Yasukawa (Yokohama National University) and Dr. Ken-ichi Akagi (Osaka University) for their help at the start of this work and Ms. Ikuko Yumen (Osaka University) for technical advice on the MALDI-TOF mass spectroscopy measurements. We are also grateful to Dr. Yoshitsugu Shiro and Dr. Midori Takeda-Sato (RIKEN SPring-8 Center) for helpful discussions about the X-ray experiments and Shunpei Nishinaka, Ryo Taniguchi, and Takashi Kakiuchi (Kyoto University, Kyoto, Japan) for the differential pulse voltammetry measurements with an MPOH-coated gold electrode and fruitful discussions.

SUPPORTING INFORMATION AVAILABLE

A table giving the chemical shifts of heme methyl signals in the five macroscopic oxidation states of mutated cyt c_3 species (Table S1), a table summarizing the reduction fractions of the four hemes at the four reduction steps (Table S2), a figure showing differential pulse polarograms and voltammograms of H22M, H25M, H35M, and H70M cyt c_3 (Figure S1), a figure showing cyclic voltammograms (CVs) of H25M and H35M cyt c_3 and peak current/(scan rate)$^{1/2}$ plots for CVs of H22M, H25M, H35M, and H70M cyt c_3 (Figure S2), and a figure showing a differential pulse polarogram of H52M cyt c_3 (Figure S3). This material is available free of charge via the Internet at http://pubs.acs.org.

REFERENCES

1. Ambler, R. P. (1980) in *From Cyclotrons to Cytochromes* (Robinson, A. B., and Kaplan, K. O., Eds.) pp 263−279,Academic Press, London.

2. Harada, E., Fukuoka, Y., Ohmura, T., Fukunishi, A., Kawai, G., Fujiwara, T., and Akutsu, H. (2002) Redox-coupled conformational alterations in cytochrome c_3 from *D. vulgaris* Miyazaki F on the basis of its reduced solution structure. *J. Mol. Biol. 319*, 767–778.
3. Akutsu, H., and Takayama, Y. (2007) Functional roles of the heme architecture and its environment in tetraheme cytochrome *c*. *Acc. Chem. Res. 40*, 171–178.
4. Kimura, K., Nakahara, Y., Yagi, T., and Inokuchi, H. (1979) Electrical conduction of hemoprotein in the solid phase: Anhydrous cytochrome c_3 film. *J. Chem. Phys. 70*, 3317–3323.
5. Takayama, Y., Harada, E., Kobayashi, R., Ozawa, K., and Akutsu, H. (2004) Roles of noncoordinated aromatic residues in redox regulation of cytochrome c_3 from *Desulfovibrio vulgaris* Miyazaki F. *Biochemistry 43*, 10859–10866.
6. Niki, K., Kobayashi, Y., and Matsuda, H. (1984) Determination of macroscopic standard potentials of a molecule with a reversible *n*-consecutive one-electron-transfer process. Application to a tetraheme protein: cytochrome c_3. *J. Electroanal. Chem. 178*, 333–341.
7. Mus-Veteau, I., Dolla, A., Guerlesquin, F., Payan, F., Czjzek, M., Haser, R., Bianco, P., Haladjian, J.-O., Rapp-Giles, B. J., and Wall, J. D. (1992) Site-directed mutagenesis of tetraheme cytochrome c_3. Modification of oxidoreduction potentials after heme axial ligand replacement. *J. Biol. Chem. 267*, 16851–16858.
8. Dolla, A., Florens, L., Bianco, P., Haladjian, J., Voordouw, G., Forest, E., Wall, J., Guerlesquin, F., and Bruschi, M. (1994) Characterization and oxidoreduction properties of cytochrome c_3 after heme axial ligand replacement. *J. Biol. Chem. 269*, 6340–6346.
9. Picarra-Pereira, M. A., Turner, D. L., LeGall, J., and Xavier, A. V. (1993) Structural studies on *Desulfovibrio gigas* cytochrome c_3 by two-dimensional ^{1}H-nuclear-magnetic-resonance spectroscopy. *Biochem. J. 294*, 909–915.
10. Morais, J., Palma, P. N., Frazão, C., Caldeira, J., LeGall, J., Moura, I., Moura, J. G., and Carrondo, M. A. (1995) Structure of the tetraheme cytochrome from *Desulfovibrio desulfuricans* ATCC 27774: X-ray diffraction and electron paramagnetic resonance studies. *Biochemistry 34*, 12830–12841.
11. Guigliarelli, B., Bertrand, P., More, C., Haser, R., and Gayda, J. P. (1990) Single-crystal electron paramagnetic resonance study of cytochrome c_3 from *Desulfovibrio desulfuricans* Norway strain. Assignment of the heme midpoint redox potentials. *J. Mol. Biol. 216*, 161–166.
12. Pieulle, L., Haladjian, J., Bonicel, J., and Hatchikian, E. C. (1996) Biochemical studies of the *c*-type cytochromes of the sulfate reducer *Desulfovibrio africanus*. Characterization of two tetraheme cytochromes c_3 with different specificity. *Biochim. Biophys. Acta 1273*, 51–61.
13. Fan, K., Akutsu, H., Kyogoku, Y., and Niki, K. (1990) Estimation of microscopic redox potentials of a tetraheme protein, cytochrome c_3 of *Desulfovibrio vulgaris*, Miyazaki F, and partial assignments of heme groups. *Biochemistry 29*, 2257–2263.
14. Park, J.-S., Ohmura, T., Kano, K., Sagara, T., Niki, K., Kyogoku, Y., and Akutsu, H. (1996) Regulation of the redox order of four hemes by pH in cytochrome c_3 from *Desulfovibrio vulgaris* Miyazaki F. *Biochim. Biophys. Acta 1293*, 45–54.
15. Higuchi, Y., Kusunoki, M., Matsuura, Y., Yasuoka, N., and Kakudo, M. (1984) Refined Structure of Cytochrome c_3 at 1.8 Å Resolution. *J. Mol. Biol. 172*, 109–139.
16. Ozawa, K., Takayama, Y., Yasukawa, F., Ohmura, T., Cusanovich, M. A., Tomimoto, Y., Ogata, H., Higuchi, Y., and Akutsu, H. (2003) Role of the aromatic ring of Tyr43 in tetraheme cytochrome c_3 from *Desulfovibrio vulgaris* Miyazaki F. *Biophys. J. 85*, 3367–3374.
17. Ozawa, K., Yasukawa, F., Fujiwara, Y., and Akutsu, H. (2001) A simple, rapid, and highly efficient gene expression system for multiheme cytochrome c. *Biosci., Biotechnol., Biochem. 65*, 185–189.
18. Moore, G. R. (1996) Haemoproteins. In *Protein Electron Transfer* (Bendall, D. S., Ed.) pp 189−216, BIOS Scientific Publishers Ltd., Oxford, U.K.
19. Takayama, Y., Kobayashi, Y., Yahata, N., Saitoh, T., Hori, H., Ikegami, T., and Akutsu, H. (2006) Specific binding of CO to tetraheme cytochrome c_3. *Biochemistry 45* (10), 3163–3169.
20. Yagi, T., and Maruyama, K. (1971) Purification and properties of cytochrome c_3 of *Desulfovibrio vulgaris*, Miyazaki. *Biochim. Biophys. Acta 243*, 214–224.
21. Hobara, D., Ota, M., Imabayashi, S., Niki, K., and Kakiuchi, T. (1998) Phase separation of binary self-assembled thiol monolayers composed of 1-hexadecanethiol and 3-mercaptopropionic acid on Au(III) studied by scanning tunneling microscopy and cyclic voltammetry. *J. Electroanal. Chem. 444*, 113–119.
22. Widrig, C. A., Chung, C., and Porter, M. C. (1991) The electrochemical desorption of n-alkanethiol monolayers from polycrystalline Au and Ag electrodes. *J. Electroanal. Chem. 310*, 335–359.
23. Park, J.-S., Kano, K., Niki, K., and Akutsu, H. (1991) Full assignment of heme redox potentials of cytochrome c_3 of *D. vulgaris* Miyazaki F by ^{1}H NMR. *FEBS Lett. 285*, 149–151.
24. Ohmura, T., Inobe, T., Kano, K., Horizumi, T., and Akutsu, H. (1997) Unusual behavior of a heme in a tetraheme protein, cytochrome c_3 from *Desulfovibrio vulgaris* Miyazaki F, in the reduction process. *J. Electroanal. Chem. 438*, 237–243.
25. Saitoh, T., Tachibana, Y., Higuchi, Y., Hori, H., and Akutsu, H. (2004) Correlation between the *g* tensors and the nonplanarity of porphyrin rings in *Desulfovibrio vulgaris* Miyazaki F cytochrome c_3, studied by single crystal EPR. *Bull. Chem. Soc. Jpn. 77*, 357–363.
26. Otwinowski, Z., and Minor, W. (1997) Processing of X-ray diffraction data collected in oscillation mode. *Methods Enzymol. 276*, 307–326.
27. Leslie, A. G. W. (1990) *MOSFILM*, version 5.41, Oxford University Press, Oxford, U.K.
28. Brünger, A. T., Adams, P. D., Clore, G. M., DeLano, W. L., Gros, P., Grosse-Kunstleve, R. W., Jiang, J.-S., Kuszewski, J., Nilges, M., Pannu, N. S., Read, R. J., Rice, L. M., Simonson, T., and Warren, G. L. (1998) Crystallography & NMR system: A new software suite for macromolecular structure determination. *Acta Crystallogr. D54*, 905–921.
29. Sheldrick, G. M., and Schneider, T. R. (1997) SHELXL: High-resolution refinement. *Methods Enzymol. 277*, 319–343.
30. Guex, N., and Peitsch, M. C. (1996) Swiss-PDBViewer: A fast and easy-to-use PDB Viewer for Macintosh and PC. *Protein Data Bank Quarterly Newsletter 77*, 7.
31. Allen, J. W. A., Leach, N., and Ferguson, S. J. (2005) The histidine of the *c*-type CXXCH haem-binding motif is essential for haem attachment by the *Eschirichia coli* cytochrome *c* maturation (Ccm) apparatus. *Biochem. J. 389*, 587–592.
32. Dolla, A., Florens, L., Bruschi, M., Dudich, I. V., and Makarov, A. A. (1995) Drastic influence of a single heme axial ligand replacement on the thermostability of cytochrome c_3. *Biochem. Biophys. Res. Commun. 211*, 742–747.
33. Akutsu, H., and Hirasawa, M. (1992) Non-equivalent natures of the coordinated imidazole rings of cytochrome c_3 from *D. vulgaris* Miyazaki F as studied by ^{1}H NMR. *FEBS Lett. 308*, 264–266.
34. Santos, H., and Turner, D. L. (1987) Proton NMR studies of horse ferricytochrome *c*. Completion of the assignment of the well resolved hyperfine shifted resonances. *FEBS Lett. 226*, 179–185.
35. Salgueiro, C. A., da Costa, P. N., Turner, D. L., Messias, A. C., van Dongen, W. M. A. M., Saraiva, L. M., and Xavier, A. V. (2001) Effect of hydrogen-bond networks in controlling reduction potentials in *Desulfovibrio vulgaris* (Hildenborough) cytochrome c_3 probed by site-specific mutagenesis. *Biochemistry 40*, 9709–9716.
36. Turkarsian, S., Sanders, C., and Daldal, F. (2006) Extracytoplasmic prosthetic group ligation to apoproteins: Maturation of c-type cytochromes. *Mol. Microbiol. 60*, 537–541.
37. Cianciotto, N. P., Cornelis, P., and Baysse, C. (2005) Impact of the bacterial type I cytochrome *c* maturation system on different biological processes. *Mol. Microbiol. 56*, 1408–1415.
38. Crow, A., Acheson, R. M., Le Brun, N. E., and Oubrie, A. (2004) Structural basis of redox-coupled protein substrate selection by the cytochrome *c* biosynthesis protein ResA. *J. Biol. Chem. 279*, 23654–23660.
39. Colbert, C. L., Wu, Q., Erbel, P. J. A., Gardner, K. H., and Deisenhofer, J. (2006) Mechanism of substrate specificity in *Bacillus subtilis* ResA, a thioredoxin-like protein involved in cytochrome *c* maturation. *Proc. Natl. Acad. Sci. U.S.A. 103*, 4410–4415.
40. Takayama, Y., Shen, Y., and Akutsu, H. (2007) Process of maturation of tetraheme cytochrome c_3 in a *Shewanella* expression system. *J. Biochem. 141*, 121–126.
41. Correia, I. J., Paquete, C. M., Louro, R. O., Catarino, T., Turner, D. L., and Xavier, A. V. (2002) Thermodynamic and kinetic characterization of trihaem cytochrome c_3 from *Desulfuromonas acetoxidans*. *Eur. J. Biochem. 269*, 5722–5730.
42. Pessanha, M., Morgado, L., Louro, R. O., Londer, Y. Y., Pokkuluri, P. R., Schiffer, M., and Salgueiro, C. A. (2006) Thermodynamic characterization of triheme cytochrome PpcA from *Geobacter*

sulfurreducens: Evidence for a role played in e^-/H^+ energy transduction. *Biochemistry 45*, 13910–13917.

43. Aubert, C., Guerlesquin, F., Bianco, P., Leroy, G., Tron, P., Stetter, K.-O., and Bruschi, M. (2001) Cytochromes c_{555} from the hyperthermophilic bacterium *Aquifex aeolicus*. 2. Heterologous production of soluble cytochrome c_{555} and investigation of the role of methionine residues. *Biochemistry 40*, 13690–13698.
44. Miller, G. T., Zhang, B., Hardman, J. K., and Timkovich, R. (2000) Converting a *c*-type to a *b*-type cytochrome: Met61 to His61 mutant of *Pseudomonas* cytochrome *c*-551. *Biochemistry 39*, 9010–9017.
45. Stellwagen, E. (1978) Haem exposure as the determinate of oxidation-reduction potential of haem proteins. *Nature 275*, 73–74.
46. Harada, E., Kumagai, J., Ozawa, K., Imabayashi, S., Tsapin, A. S., Nealson, K. H., Meyer, T. E., Cusanovich, M. A., and Akutsu, H. (2002) A directional electron transfer regulator based on heme-chain architecture in the small tetraheme cytochrome *c* from *Shewanella oneidensis*. *FEBS Lett. 532*, 333–337.
47. Sayle, R. A., and Milner-White, E. J. (1995) RASMOL: Biomolecular graphics for all. *Trends Biochem. Sci. 20*, 374–376.

BI8005708